NANO LETTERS

pubs.acs.org/NanoLett Letter

Intermolecular Charge-Transfer-Induced Strong Optical Emission from Herringbone H-Aggregates

Qi Sun, Jiajun Ren, Tong Jiang, Qian Peng, Qi Ou,* and Zhigang Shuai*

Cite This: *Nano Lett.* 2021, 21, 5394−5400 Read Online

ACCESS | Metrics & More | Article Recommendations | Supporting Information

ABSTRACT: Luminescence in molecular aggregates can be quenched either by intermolecular charge transfer or by forming a dipole-forbidden lower Frenkel exciton in H-aggregate. Taking intermolecular charge transfer and excitonic coupling into a three-state model through localized diabatization, we demonstrate that the low-lying intermolecular charge-transfer state could couple with the upper bright Frenkel exciton to form dipole-allowed S_1 that lies below the dark state, which accounts for the recent experimentally discovered strong luminescence in organic light-emitting transistors (OLETs) system with DPA and dNaAnt herringbone aggregates. The condition of forming such bright state is that the electron and hole transfer integrals, t_e and t_h, are of the same sign, and should be notably larger than the excitonic coupling (J), that is , $t_e \times t_h > 2J^2$. This theoretical finding not only rationalizes recent experiments but unravels an exciting scenario where strong luminescence and high charge mobilities become compatible, which is a preferable condition for both OLETs and electrically pumped lasing.

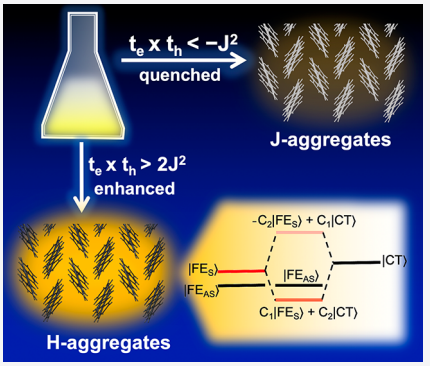

KEYWORDS: *photoluminescence quantum yield, carrier mobility, H-aggregates, OLET*

I. INTRODUCTION

Over the last two decades, promising advantages of organic light-emitting transistors (OLETs) have been significantly explored, which promote the performance of organic light-emitting and display devices.[1−8] Compared with organic light-emitting diodes (OLEDs), OLETs combine the switching abilities of a transistor that simplifies the circuitry required for display applications. Owing to its capability of providing high current density and low optical loss at the electrodes, OLET also has great potential in realizing electrically pumped organic lasers.[9,10] Nevertheless, superior OLET candidates require both strong photoluminescence and high charge mobility, which are normally considered as two contradictory properties and difficult to be simultaneously satisfied within one organic compound.[3,7,11,12] Such contradiction arises from the fact that large transfer integrals, which are essential to high charge mobility, may introduce lower-lying intermolecular charge-transfer (CT) state that quenches optical emission. Furthermore, the reported promising organic transistors to date are typically tight-packing H-aggregates rather than J-aggregates[13] of which the emission process is prohibited within the traditional Kasha's exciton model (Figure 1).[14] In addition, it is generally conceived in organic optoelectronic devices that the carrier recombination is of the Langevin-type,[15] namely, high mobility leads to fast nonradiative decay, which is detrimental to optical emission. Therefore, molecular design of OLET materials is still full of challenges.

According to Kasha's exciton model (Figure 1),[14] the lowest excited state of an H-aggregate dimer, with positive excitonic coupling J, is a dipole-forbidden antisymmetric Frenkel exciton (FE), and hence the emission is prohibited. For the J-aggregate dimer, due to a negative exciton coupling, the lowest excited state becomes dipole-allowed symmetric FE, of which the transition dipole moment is strengthened by a factor of $\sqrt{2}$ compared to that of the monomer. The emission of the J-aggregate is thus enhanced upon aggregation, which corresponds to the origin of superradiance.[16] While ubiquitously applied in organic crystalline systems, this classical Kasha picture relies on a 1D model and does not account for the effect of wave function overlaps, which is indeed essential to the photoluminescence as well as charge transport properties of the crystal. In fact, theoretical studies have shown that H- and J-aggregate properties can simultaneously exist within one crystalline structure depending on the choice of the aggregating direction, and the one with stronger exciton coupling is usually experimentally observed. Moreover, such property can be altered by a number of factors such as the change of temperature[17] and the involvement of CT exciton

Received: May 5, 2021
Revised: June 9, 2021
Published: June 14, 2021

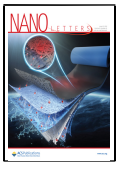

https://doi.org/10.1021/acs.nanolett.1c01734
Nano Lett. 2021, 21, 5394−5400

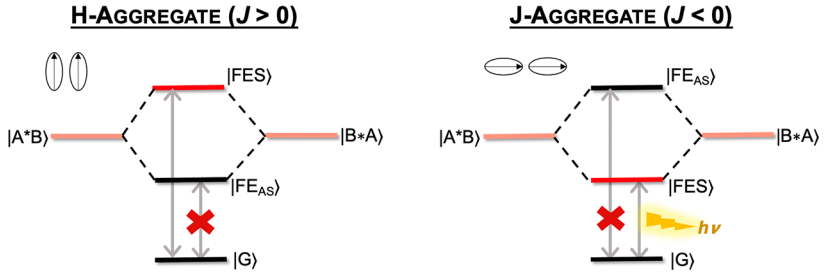

Figure 1. Schematic exciton coupling model for conventional Kasha H- and J-aggregate dimers. The transition dipole moments of each monomer point to the same direction, giving rise to the dipole-allowed symmetric FE ($|FE_S\rangle$) and dipole-forbidden antisymmetric FE ($|FE_{AS}\rangle$). The strength of the transition dipole moment is denoted by the saturation of the red color: $|FE_S\rangle$ has larger transition dipole moment compared to the excited states of each monomer $|A^*B\rangle$ and $|B^*A\rangle$, and the black color corresponds to dipole-forbidden dark states.

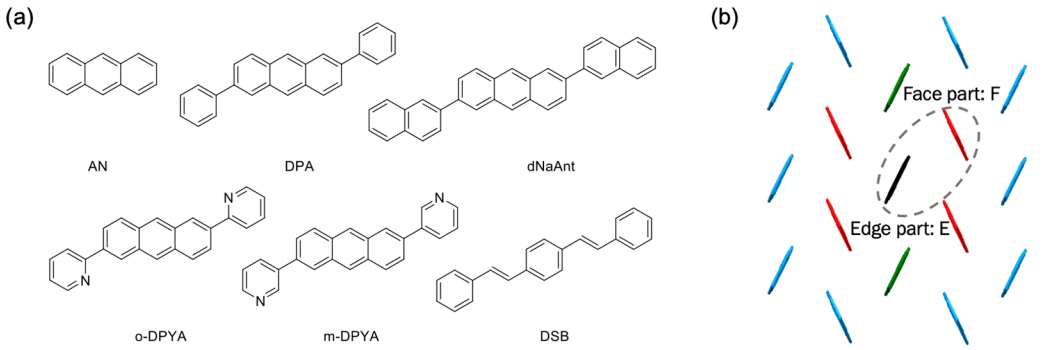

Figure 2. (a) Molecular structures of HB aggregates investigated in this work. (b) Schematic HB packing motif.

(CTE),[18−22] which would essentially affect the energetic order of the excited states. While previous theoretical works mainly focus on π-stacking aggregates via means of parametrized model Hamiltonians and/or modeled aggregate systems,[19,20,23] the luminescence mechanism of herringbone (HB) packing motif remains unclear, of which the characteristic is different from its π-stacking counterpart. More importantly, to address the aforementioned entangled factors, a quantitative description directly from *ab initio* calculation for the luminescence mechanism of realistic crystalline aggregates is undoubtedly desired.

Keeping these in mind, we focus on various HB aggregates (Figure 2a) in this work and propose a quantitative description of their photoluminescence mechanism through a diabatic Hamiltonian constructed from Boys localized diabatization method.[24] Our calculations evince that one CTE of the investigated dimers lies closely to the FEs and presumably gets involved in the light-emitting process. On the basis of a three-state diabatic Hamiltonian, we demonstrate that the CTE would couple with the symmetric FE and form a dipole-allowed S_1 in H-aggregates if the electron and hole transfer integrals are of the same sign and their strength is notably larger than the exciton coupling. This hybrid S_1 state lies below the dark state and benefits the fluorescent process. In principle, larger transfer integrals also benefit charge mobility. We further investigate the role played by the packing configurations in the light-emitting properties for anthracene derivatives, and screen out favored packing configurations for strong luminescence. Altogether, by reconciling the two conventionally contradictory factors in OLET, that is, photoluminescence and charge mobility, our theoretical protocols presented here are expected to considerably broaden the aperture of novel OLET design in the future.

II. RESULTS

A. Three-State Model Hamiltonian. In two-dimensional HB lattice, four face-to-edge stacking dimers, and two slipped $\pi-\pi$ stacking dimers can be formed between one molecule and its nearest neighbors (Figure 2b). We choose the face-to-edge stacking dimer with the shortest centroid distance and compare its properties with those of the slipped $\pi-\pi$ stacking dimer. As shown in Figure S1a, the intermolecular dispersion predicted by XSAPT+MBD[25] in face-to-edge dimers is consistently stronger than that in slipped $\pi-\pi$ stacking dimers for all investigated aggregates. Moreover, according to the point-dipole approximation, the exciton coupling J is inversely proportional to the cube of the centroid distance between two monomers. Therefore, the face-to-edge stacking dimers have stronger exciton coupling compared to slipped $\pi-\pi$ stacking dimers due to shorter centroid distances (as demonstrated in Table S1 for DSB[26]). As a result, the face-to-edge stacking dimer, which has stronger intermolecular interaction and exciton coupling compared to the slipped $\pi-\pi$ counterpart, is expected to exhibit more pronounced aggregation effect and therefore is employed to investigate the luminescence properties of the aggregates.

Within one face-to-edge stacking dimer, two types of CTE are formed, which are denoted as F^+E^- (charge transferred from "face" part to "edge" part) and F^-E^+ (charge is transferred from "edge" part to "face" part). (See Figure 2b for the definitions of the "face" and "edge" parts.) The excitation energies of F^-E^+ and F^+E^- for all investigated systems (based on an isolated dimer) are shown in Table 1, together with the S_1 excitation energies of monomers for comparison. It can be seen that F^-E^+ is significantly lower in energy than F^+E^- and lies closely to the locally excited S_1 state. Such energetic separation can be attributed to different intermolecular

https://doi.org/10.1021/acs.nanolett.1c01734
Nano Lett. 2021, 21, 5394−5400

Table 1. Excitation Energy of the Two Types of CTEs and Locally Excited S_1 State of the Monomer in Face-to-Edge Dimers Computed from Boys Localized Diabatization Method at the Level of ωB97X-D*/6-31G(d)[a]

compound	$E_{F^-E^+}$	$E_{F^+E^-}$	E_{S_1}
An	4.05	4.79	3.64
DPA	3.38	4.16	3.32
dNaAnt	3.25	4.07	3.26
o-DPYA	3.49	4.20	3.41
m-DPYA	3.63	4.20	3.39
DSB	4.00	4.73	3.83/3.92[b]

[a]Numbers are shown in the unit of eV. [b]Two locally excited states have different energies.

interactions inside these two CTEs. As shown in Figure S1b and Table S2, the overall attraction inside F^-E^+ is stronger than that inside F^+E^-, which mainly results from larger electrostatic and induction forces. Such stronger attraction stabilizes the energy of F^-E^+, making it energetically possible for F^-E^+ (rather than F^+E^-) to couple with the locally excited states of the monomer. While previous study has reported that such energetic separation in pentacene dimer can be strongly decreased when taking the actual crystalline environment into consideration,[27] we find that a pure F^+E^- state can be obtained from the QM/MM method[28,29] for our investigated aggregates (as shown in Figure S2) and its energy is significantly higher than those of the first three adiabatic excited state (as shown in Table S3), which reinforces that F^+E^- is unlikely to couple with low-lying locally excited states of these systems.

Since only one CTE (F^-E^+) is energetically favorable to couple with the locally excited state of each monomer (denoted as F*E and FE* for consistency) for HB aggregates investigated in this work, their electronic structure and photophysical properties can be comprehensively described via a three-state diabatic Hamiltonian. Within Boys localized diabatization algorithm,[24] the charge separation of each diabatic state ($|F^*E\rangle$, $|FE^*\rangle$, and $|F^-E^+\rangle$) is maximized, and the diabatic Hamiltonian in the basis of $\{\{|F^*E\rangle; |FE^*\rangle; |F^-E^+\rangle\}$ is of the form

$$\hat{H} = \begin{bmatrix} E & J & t_h \\ J & E & t_e \\ t_h & t_e & E_{CT} \end{bmatrix} \quad (1)$$

where E is the excitation energy of the locally excited state of each monomer; E_{CT} is the excitation energy of F^-E^+. $\hat{H}$ can further be represented on the basis of $\{|FE_{AS}\rangle; |FE_S\rangle; |F^-E^+\rangle\}$ (denoted as $\hat{\mathcal{H}}$) as

$$\hat{\mathcal{H}} = \begin{bmatrix} E-J & 0 & \frac{\sqrt{2}}{2}(t_h - t_e) \\ 0 & E+J & \frac{\sqrt{2}}{2}(t_h + t_e) \\ \frac{\sqrt{2}}{2}(t_h - t_e) & \frac{\sqrt{2}}{2}(t_h + t_e) & E_{CT} \end{bmatrix} \quad (2)$$

To unravel the luminescence mechanism of the aggregates, one needs to diagonalize $\hat{\mathcal{H}}$ and explicitly analyze the resulting eigenstates as well as the eigenenergies, of which the expression is tediously long without any approximation and impractical to be employed for our analysis. Therefore, we perform the diagonalization within two simplified but practical scenarios, (i) $t_h \approx t_e = t$ and (ii) $t_h \approx -t_e = t$. For $t_h \approx t_e = t$, the first two eigenenergies are given by

$$E_1 = E - J \quad (3)$$

$$E_2 = E + \frac{s + J - \sqrt{(s-J)^2 + 8t^2}}{2} \quad (4)$$

where $s = E_{CT} - E$; with the corresponding eigenstates

$$\Psi_1 = |FE_{AS}\rangle \quad (5)$$

$$\Psi_2 = \frac{1}{\sqrt{C^2+1}}(C|FE_S\rangle + |F^-E^+\rangle) \quad (6)$$

where $C = E_{CT} - E - J + \sqrt{(E_{CT} - E - J)^2 + 8t^2}$. It can be seen from eqs 5 and 6 that when $t_h \approx t_e = t$, CTE mainly couples with symmetric FE, that is, the bright state with μ_F and μ_E pointing to the same direction, while the antisymmetric FE remains unchanged. Such expression holds for both H-aggregate ($J > 0$) and J-aggregate ($J < 0$). For H-aggregates (as schematically shown in Figure 3a), if the coupling between

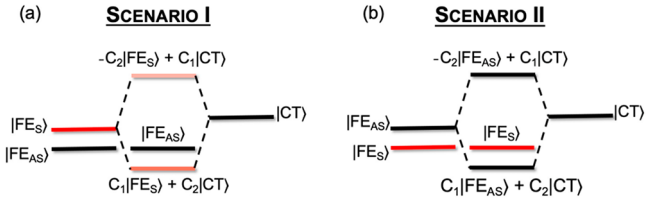

Figure 3. Schematic graph of the eigenstates of $\hat{\mathcal{H}}$ for (a) scenario I ($t_h \approx t_e = t$ for H-aggregates) and (b) scenario II ($t_h \approx -t_e = t$ for J-aggregates). $C_1 = C/\sqrt{C^2+1}$, $C_2 = 1/\sqrt{C^2+1}$. The strength of the transition dipole moment is denoted by the saturation of the red color: the state with more saturated red color has a larger transition dipole moment, and the black color corresponds to dipole-forbidden dark states.

$|FE_S\rangle$ and $|F^-E^+\rangle$ is large enough, Ψ_2, which is a partially bright state, might lie below Ψ_1 and become the light-emitting state. The emission process in such a case will no longer be prohibited, leading to the breakdown of the traditional Kasha picture for H aggregates. Furthermore, when $|FE_S\rangle$ is lower in energy than $|F^-E^+\rangle$, that is, $E + J < E_{CT}$, the contribution of $|FE_S\rangle$ to Ψ_2 will exceed 50%, and the resulting transition dipole moment of Ψ_2 (the lowest excited (light-emitting) state) will be enhanced compared to that of the monomer. Such an enhancement can be realized when $|t| > \sqrt{2}|J|$, which corresponds to the minimal requirement for $E_2 < E_1$ and $E + J < E_{CT}$. In other words, the H-aggregates may exhibit an enhanced emission process with a red-shifted emission peak compared to the monomer, which conventionally appears in J-aggregates, under the condition that the hole and electron transfer integrals are of the same sign ($t_h \approx t_e = t$) and their values are noticeably larger than the exciton coupling ($|t| > \sqrt{2}|J|$). It should be noted that such conversion from H- to J-aggregates was originally proposed in ref 19 for a different situation in which the two CTEs are degenerate. If the same condition is met in J-aggregates, the traditional Kasha picture

https://doi.org/10.1021/acs.nanolett.1c01734
Nano Lett. 2021, 21, 5394−5400

will hold and light emission will be enhanced just as that in normal J-aggregates.

Conversely, for the second scenario CTE mainly couples to the dark $|FE_{AS}\rangle$, while the bright $|FE_S\rangle$ remains unchanged, as demonstrated by the eigenstates of $\hat{H}$ in the Supporting Information. The lowest excited state of H-aggregates in such a case will always be dark since it is a linear combination of two dipole-forbidden states, $|FE_{AS}\rangle$ and $|F^-E^+\rangle$, that is, the traditional Kasha picture will hold. For J-aggregates, in which $|FE_{AS}\rangle$ lies above $|FE_S\rangle$, the emission processes will be quenched if t_e or t_h is larger than $|J|$ and the hybrid dark state becomes the lowest excited state (as schematically illustrated in Figure 3b). Therefore, $t_h \times t_e < 0$ is a presumably detrimental condition for strong luminescence upon aggregation.

B. Application of the Three-State Model to Realistic Systems. To carry out quantitative analysis for HB aggregates investigated in this work, we choose DPA[30] as a representative and its attachment-detachment densities of three localized diabatic states are shown in Figure 4. Explicit matrix elements

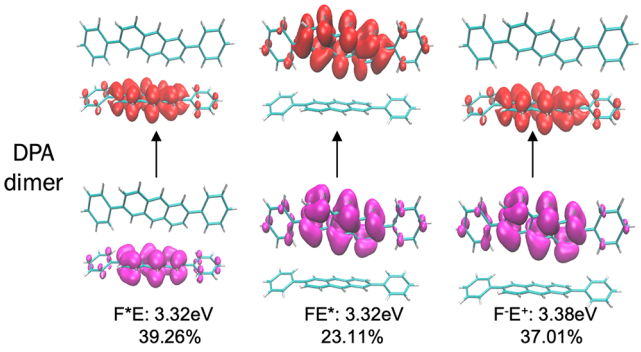

Figure 4. Attachment−detachment densities and excitation energies of the resulting diabatic states, FE*, F*E, and F^-E^+ of DPA. The percentages listed below the excitation energy are the contribution of the corresponding diabatic state to the adiabatic S_1 state of DPA.

of the diabatic Hamiltonian and the adiabatic-to-diabatic rotation matrix as well as the attachment−detachment densities of the diabatic states for the rest of systems can be found in Table S4 and Figure S3, respectively. From the attachment−detachment densities, three diabatic states, $|F^*E\rangle$, $|FE^*\rangle$, and $|F^-E^+\rangle$, are successfully constructed for each compound. The calculated exciton couplings, which correspond to the value of the matrix element H_{12}, are all positive, indicating that these face-to-edge dimers should be identified as H-aggregates in a conventional Kasha picture. The transfer integrals and exciton couplings of the investigated systems are also calculated via fragment molecular orbital method (Table S5), and the resulting values are in good agreement with those given by the localized diabatization method, which rationalizes the diabatization process.

From the calculated results, the condition for converting H-aggregates to J-aggregates ($|t| > \sqrt{2}|J|$, i.e., the first scenario), is met in DPA,[30] AN,[31] and dNaAnt[32] dimers, and the radiative decay rate k_r of the aggregates is thus expected to be increased compared to that of the isolated molecules. Note that even though DSB falls into the first scenario, its transfer integrals are significantly smaller compared to its exciton coupling, and hence $|FE_{AS}\rangle$ remains to be the lowest excited state, making it a traditional Kasha H-aggregate that the radiative decay rate will be decreased upon aggregation. Contrarily, t_h and t_e are of the opposite sign in o-DPYA and m-DPYA,[33] which fall into the second scenario where the CTE couples with dark FE, and the emission is expected to be prohibited. We compare our predicted change of k_r upon aggregation with experimental observations for these investigated systems in Table 2. It can be seen that the theoretical

Table 2. Exciton Couplings (J) and Transfer Integrals (t_h, t_e) Evaluated via Boys Localized Diabatization Method for All Investigated Systems.[a]

compound	J	t_h	t_e	k_r (theor)	k_r (exp)
An[31]	8	32	69	↑	↑
DPA[30]	12	76	62	↑	↑
dNaAnt[32]	26	60	66	↑	↑
o-DPYA[33]	7	93	−36	↓	↓
m-DPYA[33]	6	78	−41	↓	↓
DSB[26]	80	2	20	↓	↓

[a]Numbers are shown in the unit of meV. The theoretical predicted and experiment observed change of k_r upon aggregation are also listed.

predictions are in perfect agreement with experiments, which rationalize our applied three-state model Hamiltonian. It should be noted that DPA has been previously assigned as J-aggregate due to the enhanced and red-shifted emission experimentally observed in crystal.[30] This is not necessarily correct since the theoretically predicted exciton coupling for DPA is positive. On the basis of our theoretical investigations here, the enhancement and the red shift in the absorption process upon aggregation are more possibly contributed from the mediation of the CTE.

Our three-state model Hamiltonian can be further validated via the QM/MM excited state calculations of which one face-to-edge dimer is treated as the QM part. From Table S6, the calculated transition dipole moments of AN, DPA, and dNaAnt exhibit comparable or even larger magnitude compared to their monomer counterparts, while those of o-DPYA, m-DPYA, and DSB are considerably decreased upon aggregation. These QM/MM results are consistent with what we have concluded from the three-state diabatic Hamiltonian. The significance and rationality of the diabatic Hamiltonian not only rely on the resulting correct electronic structure properties, but indeed on the unraveled insights of the CT-enhanced strong emission mechanism of H-aggregates, which cannot be disclosed by the direct QM/MM calculation.

C. Screening out Favored Packing Motif for Strong Luminescence. From the above discussion, the relative sign of the electron and hole transfer integrals is essential to the luminescence properties of the aggregates. While the CTE is beneficial to the emission processes in H-aggregates when $t_h \times t_e > 0$, it will presumably quench the emission in J-aggregates if $t_h \times t_e < 0$ and the absolute value of t_h and t_e is significantly larger than that of the exciton coupling. Therefore, it is of significant importance to explore the relationship between the explicit crystal structure and the relative sign of t_h and t_e so as to quickly screen out the light-emitting favored systems.

Taking DPA as an example, in Figure 5a,b, we plot two possible configurations of the dimer, depending on the orientation of the 2-fold screw rotation axis $\hat{S}_2$ (colored in blue in Figure 5a,b). In anthracene derivatives studied in this work, An, DPA, and dNaAnt are eclipsed dimers, of which t_h

https://doi.org/10.1021/acs.nanolett.1c01734
Nano Lett. 2021, 21, 5394−5400

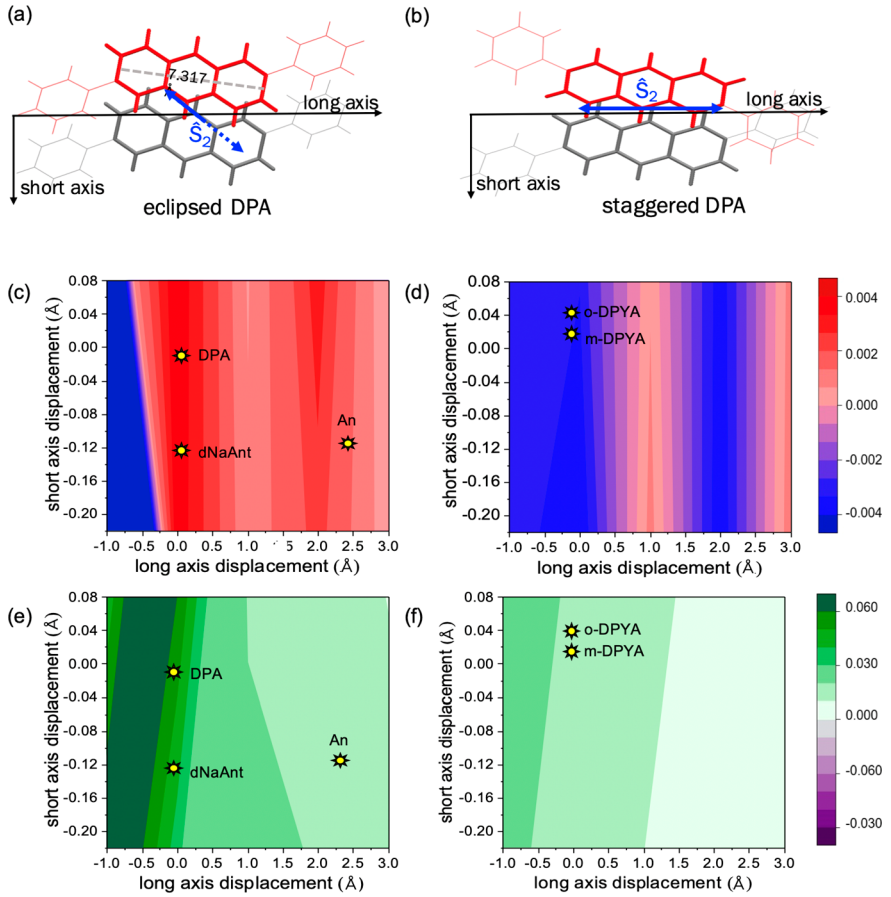

Figure 5. Two packing motifs and the influence of the packing motif to transfer integral and exciton coupling. Panels a,b correspond to the structure of eclipsed and staggered DPA face-to-edge dimers; panels c and e correspond to the calculated $t_h \times t_e$ (in unit of eV^2) and J (in unit of eV) of the eclipsed DPA dimer with respect to the displacements along the short and long axes; panels d and f correspond to those of the staggered DPA dimer.

and t_e are of the same sign, while the remaining two systems are staggered dimers of which t_h and t_e have opposite signs. The eclipsed structures are seemingly profitable to the photoluminescence. Nevertheless, caution has to been taken when exploring the dependence of the transfer integrals to the crystals structure, as previous studies have demonstrated that the signs of transfer integrals might be changed depending on the node distribution of the frontier orbitals and the displacement between two monomers.[34]

To make a more solid connection between the crystal structure and the transfer integrals, we construct the eclipsed and staggered configurations of the face-to-edge dimers of DPA, and slip one of the monomers along the short and long axes (Figure 5a,b) and calculate the transfer integral at various slipping coordinates. The rationality of such modeled packing structure lies in the fact that the frontier orbitals of these five anthracene derivates mainly localize on the anthracene moiety with almost identical node distributions (Figure S4). Note that the distance along the third direction is fixed, since it will only influence the strength of the transfer integrals and the exciton coupling but not their relative signs. The displacement along the long axis is set to be −1.00∼3.00 Å, while the one along the short axis is set to be −0.22∼0.08 Å according to the practical packing structure of anthracene derivatives studied in this work. As shown in Figure 5c,d, nearly opposite behaviors of the relative sign of t_h and t_e are found in eclipsed and staggered dimers within the displacement region while the exciton coupling is consistently positive (Figure 5e,f), indicating the contrary role played by CTE in these two packing configurations. Moreover, the sign of $t_h \times t_e$ remains unchanged in both eclipsed dimers or staggered dimers when we change the herringbone angle from 40° to 60° by rotating one of the molecules, which covers the range of the herringbone angles for all investigated systems (Figure S5). Altogether, these findings reinforce that when a low-lying CTE couples with FEs in HB H-aggregates of anthracene derivatives, the eclipsed stacking configurations tend to exhibit enhanced k_r in crystals because the sign of $t_h \times t_e$ is generally positive for a wide range of modeled packing structures. On the contrary, t_h and t_e tend to be opposite signed and/or small in staggered stacking configurations, and therefore staggered packing configurations are unfavorable for light-emitting crystals and the design of OLET materials. Modeled packing structures with larger displacements have also been investigated in Figure S6, and the resulting signs of $t_h \times t_e$ and the exciton coupling can be employed as a quick predictor to evaluate the photoluminescence and charge transport properties for a variety of anthracene derivatives.

III. DISCUSSION AND CONCLUSION

To conclude, we have proposed a promising scenario to achieve high luminescence as well as presumably high charge mobilities for HB H-aggregates with the aid of intermolecular charge transfer. We have comprehensively analyzed the nature

https://doi.org/10.1021/acs.nanolett.1c01734
Nano Lett. 2021, 21, 5394−5400

of the lowest-lying excited state in six HB H-aggregates via a three-state diabatic Hamiltonian that quantitatively unravels the emission mechanism of the investigated H-aggregates. When the electron and hole transfer integrals are of the same sign ($t_h \approx t_e = t$) and their absolute values are notably larger than that of the exciton coupling ($|t| > \sqrt{2}|J|$), the intermolecular CTE strongly couples with the bright FE and forms a dipole-allowed S_1, which lies below the dark state and may enable strong luminescence. Such enhanced luminescence behavior, which is traditionally recognized as the hallmark of the J-aggregates, is thus attained in H-aggregates with considerable transfer integrals. Since large transfer integrals are also favored by high charge mobilities, the photoluminescence and charge transport become compatible in this scenario. Therefore, H aggregates with $t_h \times t_e > 0$ are advantageous OLET candidates, of which the photoluminescence and charge transport are indeed compatible. By properly slipping one of the monomers along the short and long axes, we have explored the sign of $t_h \times t_e$ within the practical packing range of anthracene derivatives and find out that the eclipsed configuration almost always has positive $t_h \times t_e$, thus becoming a favored configuration for OLETs.

In summary, the tacit mechanism of the intermolecular CT-induced strong emission in HB H-aggregates has been explicitly disclosed in this work, which demonstrates an OLET-favored scenario where the photoluminescence and charge mobility are not mutually exclusive but compatible with each other. Looking forward, our theoretical protocol presented here would promise more advanced OLET materials with brighter emission and higher mobilities in the future.

■ ASSOCIATED CONTENT

Supporting Information

The Supporting Information is available free of charge at https://pubs.acs.org/doi/10.1021/acs.nanolett.1c01734.

Methods and computational details applied in this work, mathematical derivation of scenario II, intermolecular interactions of F^-E^+ and F^+E^-, additional attachment−detachment densities, diabatic Hamiltonians and rotation matrix obtained from 3-state Boys localized diabatization, calculated $t_h^* t_e$ and J of the eclipsed and staggered DPA face-to-edge dimers with respect to the herringbone angles as well as a larger displacement along the short and long axis, Figures S1−S6 and Tables S1−S6 (PDF)

■ AUTHOR INFORMATION

Corresponding Authors

Qi Ou − *MOE Key Laboratory of Organic OptoElectronics and Molecular Engineering, Department of Chemistry, Tsinghua University, Beijing 100084, P.R. China*; Email: zgshuai@tsinghua.edu.cn

Zhigang Shuai − *MOE Key Laboratory of Organic OptoElectronics and Molecular Engineering, Department of Chemistry, Tsinghua University, Beijing 100084, P.R. China*; orcid.org/0000-0003-3867-2331; Email: qiou@tsinghua.edu.cn

Authors

Qi Sun − *MOE Key Laboratory of Organic OptoElectronics and Molecular Engineering, Department of Chemistry, Tsinghua University, Beijing 100084, P.R. China*

Jiajun Ren − *MOE Key Laboratory of Organic OptoElectronics and Molecular Engineering, Department of Chemistry, Tsinghua University, Beijing 100084, P.R. China*; orcid.org/0000-0002-1508-4943

Tong Jiang − *MOE Key Laboratory of Organic OptoElectronics and Molecular Engineering, Department of Chemistry, Tsinghua University, Beijing 100084, P.R. China*; orcid.org/0000-0002-5907-4886

Qian Peng − *School of Chemical Sciences, University of Chinese Academy of Sciences, Beijing 100049, P.R. China*; orcid.org/0000-0001-8975-8413

Complete contact information is available at: https://pubs.acs.org/10.1021/acs.nanolett.1c01734

Author Contributions

Z.S. and Q.O. conceived the project. Q.S. carried out the calculations. Q.P., J.R., and T.J. helped with the calculation process and provided inspiring suggestions for improvement. All authors contributed to data analysis and writing the paper.

Notes

The authors declare no competing financial interest.

■ ACKNOWLEDGMENTS

This work was supported by the National Natural Science Foundation of China Grants 21788102 and 22003030, as well as by the Ministry of Science and Technology of China through the National Key R&D Plan, Grant 2017YFA0204501. Q.O. is also funded by China Postdoctoral Science Foundation Grant 2020M670280. Q.O. and J.R. are also supported by the Shuimu Tsinghua Scholar Program. The authors thank Dr. Lang Jiang for inspiring conversations.

■ REFERENCES

(1) Capelli, R.; Toffanin, S.; Generali, G.; Usta, H.; Facchetti, A.; Muccini, M. Organic light-emitting transistors with an efficiency that outperforms the equivalent light-emitting diodes. *Nat. Mater.* **2010**, *9*, 496−503.

(2) Zhang, C.; Chen, P.; Hu, W. Organic Light-Emitting Transistors: Materials, Device Configurations, and Operations. *Small* **2016**, *12*, 1252−1294.

(3) Yuan, D.; Sharapov, V.; Liu, X.; Yu, L. Design of High-Performance Organic Light-Emitting Transistors. *ACS Omega* **2020**, *5*, 68−74.

(4) Park, S. K.; Kim, J. H.; Ohto, T.; Yamada, R.; Jones, A. O. F.; Whang, D. R.; Cho, I.; Oh, S.; Hong, S. H.; Kwon, J. E.; Kim, J. H.; Olivier, Y.; Fischer, R.; Resel, R.; Gierschner, J.; Tada, H.; Park, S. Y. Highly Luminescent 2D-Type Slab Crystals Based on a Molecular Charge-Transfer Complex as Promising Organic Light-Emitting Transistor Materials. *Adv. Mater.* **2017**, *29*, 1701346.

(5) Zambianchi, M.; Benvenuti, E.; Bettini, C.; Zanardi, C.; Seeber, R.; Gentili, D.; Cavallini, M.; Muccini, M.; Biondo, V.; Soldano, C.; Generali, G.; Toffanin, S.; Melucci, M. Anthracene-based molecular emitters for non-doped deep-blue organic light emitting transistors. *J. Mater. Chem. C* **2016**, *4*, 9411−9417.

(6) Orgiu, E.; Samori, P. 25th anniversary article: organic electronics marries photochromism: generation of multifunctional interfaces, materials, and devices. *Adv. Mater.* **2014**, *26*, 1827−1845.

(7) Chaudhry, M. U.; Muhieddine, K.; Wawrzinek, R.; Sobus, J.; Tandy, K.; Lo, S. C.; Namdas, E. B. Organic Light-Emitting Transistors: Advances and Perspectives. *Adv. Funct. Mater.* **2020**, *30*, 1905282.

(8) Wan, Y.; Deng, J.; Wu, W.; Zhou, J.; Niu, Q.; Li, H.; Yu, H.; Gu, C.; Ma, Y. Efficient Organic Light-Emitting Transistors Based on High-Quality Ambipolar Single Crystals. *ACS Appl. Mater. Interfaces* **2020**, *12*, 43976−43983.

(9) Samuel, I. D.; Turnbull, G. A. Organic semiconductor lasers. *Chem. Rev.* **2007**, *107*, 1272−1295.
(10) Liu, D.; De, J.; Gao, H.; Ma, S.; Ou, Q.; Li, S.; Qin, Z.; Dong, H.; Liao, Q.; Xu, B.; Peng, Q.; Shuai, Z.; Tian, W.; Fu, H.; Zhang, X.; Zhen, Y.; Hu, W. Organic Laser Molecule with High Mobility, High Photoluminescence Quantum Yield, and Deep-Blue Lasing Characteristics. *J. Am. Chem. Soc.* **2020**, *142*, 6332−6339.
(11) Lee, S.; Lee, H. J.; Ji, Y.; Lee, K. H.; Hong, K. Electrochemiluminescent Transistors: A New Strategy toward Light-Emitting Switching Devices. *Adv. Mater.* **2021**, *33*, 2005456.
(12) Sun, Y.; Geng, H.; Peng, Q.; Shuai, Z. Computational Study on the Charge Transport and Optical Spectra of Anthracene Derivatives in Aggregates. *ChemPhysChem* **2020**, *21*, 952−957.
(13) Wang, C.; Dong, H.; Hu, W.; Liu, Y.; Zhu, D. Semiconducting pi-conjugated systems in field-effect transistors: a material odyssey of organic electronics. *Chem. Rev.* **2012**, *112*, 2208−2267.
(14) Kasha, M. Energy Transfer Mechanisms and the Molecular Exciton Model for Molecular Aggregates. *Radiat. Res.* **1963**, *20*, 55−71.
(15) Langevin, P. The recombination and mobilities of ions in gases. *Ann. Chim. Phys.* **1903**, *28*, 433−530.
(16) Fidder, H.; Knoester, J.; Wiersma, D. A. Superradiant Emission and Optical Dephasing in J-Aggregates. *Chem. Phys. Lett.* **1990**, *171*, 529−536.
(17) Chuang, C.; Bennett, D. I. G.; Caram, J. R.; Aspuru-Guzik, A.; Bawendi, M. G.; Cao, J. Generalized Kasha's Model: T-Dependent Spectroscopy Reveals Short-Range Structures of 2D Excitonic Systems. *Chem.* **2019**, *5*, 3135−3150.
(18) Hestand, N. J.; Spano, F. C. Expanded Theory of H- and J-Molecular Aggregates: The Effects of Vibronic Coupling and Intermolecular Charge Transfer. *Chem. Rev.* **2018**, *118*, 7069−7163.
(19) Hestand, N. J.; Spano, F. C. Molecular Aggregate Photophysics beyond the Kasha Model: Novel Design Principles for Organic Materials. *Acc. Chem. Res.* **2017**, *50*, 341−350.
(20) Yamagata, H.; Pochas, C. M.; Spano, F. C. Designing J- and H-aggregates through wave function overlap engineering: applications to poly(3-hexylthiophene). *J. Phys. Chem. B* **2012**, *116*, 14494−14503.
(21) Song, J.; Gao, F.; Shi, B.; Liang, W. Identification of the mechanism of enhanced exciton interaction in rigidly linked naphthalene dimers. *Phys. Chem. Chem. Phys.* **2010**, *12*, 13070−13075.
(22) Pan, F.; Gao, F.; Liang, W.; Zhao, Y. Nature of low-lying excited states in H-aggregated perylene bisimide dyes: results of TD-LRC-DFT and the mixed exciton model. *J. Phys. Chem. B* **2009**, *113*, 14581−14587.
(23) Hestand, N. J.; Spano, F. C. Interference between Coulombic and CT-mediated couplings in molecular aggregates: H- to J-aggregate transformation in perylene-based pi-stacks. *J. Chem. Phys.* **2015**, *143*, 244707.
(24) Subotnik, J. E.; Yeganeh, S.; Cave, R. J.; Ratner, M. A. Constructing diabatic states from adiabatic states: extending generalized Mulliken-Hush to multiple charge centers with boys localization. *J. Chem. Phys.* **2008**, *129*, 244101.
(25) Carter-Fenk, K.; Lao, K. U.; Liu, K. Y.; Herbert, J. M. Accurate and Efficient ab Initio Calculations for Supramolecular Complexes: Symmetry-Adapted Perturbation Theory with Many-Body Dispersion. *J. Phys. Chem. Lett.* **2019**, *10*, 2706−2714.
(26) Varghese, S.; Park, S. K.; Casado, S.; Fischer, R. C.; Resel, R.; Milian-Medina, B.; Wannemacher, R.; Park, S. Y.; Gierschner, J. Stimulated Emission Properties of Sterically Modified Distyrylbenzene-Based H-Aggregate Single Crystals. *J. Phys. Chem. Lett.* **2013**, *4*, 1597−1602.
(27) Petelenz, P.; Snamina, M.; Mazur, G. Charge-Transfer States in Pentacene: Dimer versus Crystal. *J. Phys. Chem. C* **2015**, *119*, 14338−14342.
(28) Dapprich, S.; Komaromi, I.; Byun, K.S.; Morokuma, K.; Frisch, M. J A new ONIOM implementation in Gaussian98. Part I. The calculation of energies, gradients, vibrational frequencies and electric field derivatives. *J. Mol. Struct.: THEOCHEM* **1999**, *461-462*, 1−21.
(29) Maseras, F.; Morokuma, K. Imomm - a New Integrated Ab-Initio Plus Molecular Mechanics Geometry Optimization Scheme of Equilibrium Structures and Transition-States. *J. Comput. Chem.* **1995**, *16*, 1170−1179.
(30) Liu, J.; Zhang, H.; Dong, H.; Meng, L.; Jiang, L.; Jiang, L.; Wang, Y.; Yu, J.; Sun, Y.; Hu, W.; Heeger, A. J. High mobility emissive organic semiconductor. *Nat. Commun.* **2015**, *6*, 10032.
(31) Katoh, R.; Suzuki, K.; Furube, A.; Kotani, M.; Tokumaru, K. Fluorescence Quantum Yield of Aromatic Hydrocarbon Crystals. *J. Phys. Chem. C* **2009**, *113*, 2961−2965.
(32) Li, J.; Zhou, K.; Liu, J.; Zhen, Y.; Liu, L.; Zhang, J.; Dong, H.; Zhang, X.; Jiang, L.; Hu, W. Aromatic Extension at 2,6-Positions of Anthracene toward an Elegant Strategy for Organic Semiconductors with Efficient Charge Transport and Strong Solid State Emission. *J. Am. Chem. Soc.* **2017**, *139*, 17261−17264.
(33) Liu, J.; Zhu, W.; Zhou, K.; Wang, Z.; Zou, Y.; Meng, Q.; Li, J.; Zhen, Y.; Hu, W. Pyridyl-substituted anthracene derivatives with solid-state emission and charge transport properties. *J. Mater. Chem. C* **2016**, *4*, 3621−3627.
(34) Kazmaier, P. M.; Hoffmann, R. A Theoretical Study of Crystallochromy. Quantum Interference Effects in the Spectra of Perylene Pigments. *J. Am. Chem. Soc.* **1994**, *116*, 9684−9691.

https://doi.org/10.1021/acs.nanolett.1c01734
Nano Lett. 2021, 21, 5394−5400